International Journal of Research
Available at https://edupediapublications.org/journals
p-ISSN: 2348-6848
e-ISSN: 2348-795X
Volume 04 Issue 02
February 2017

An Adaptive Power Oscillation Damping Controller by STATCOM With Energy Storage

SHAIK MOHAMAD RAFI & VORUGANTI BHARATH KUMAR

Guide name :MAHAMAD SAMREEN SULTHANA

Sana Engineering College, Kodad, Telangana, India

***Abstract*—The proposed method is effective in increasing the damping of the system at the frequencies of interest, also in the case of system parameter uncertainties and at various connection points of the compensator. First, the analysis of the im-pact of active and reactive power injection into the power system will be carried out using a simple two-machine system model. A control strategy that optimizes active and reactive power injection at various connection points of the STATCOM will be derived using the simplified model. Small-signal analysis of the dynamic performance of the proposed control strategy will be carried out. The effectiveness of the proposed control method to provide power oscillation damping irrespective of the connection point of the device and in the presence of system parameter uncertainties will be verified through simulation and experimental results.**

***Index Terms*—Energy storage, low-frequency oscillation, power oscillation damping (POD), recursive least square (RLS), static synchronous compensator (STATCOM).**

I. Introduction

STATIC synchronous compensator (STATCOM) is a key device for reinforcement of the stability in an ac power system. This device has been applied both at distribution level to mitigate power quality phenomena and at transmission level for voltage control and power oscillation damping (POD) [1]–[3]. Although typically used for reactive power injection only, by equipping the STATCOM with an energy storage connected to the dc-link of the converter, a more flexible control of the trans-mission system can be achieved [4], [5]. An installation of a STATCOM with energy storage is already found in the U.K. for power flow management and voltage control [6]. The in-troduction of wind energy and other distributed generation will pave the way for more energy storage into the power system and auxiliary stability enhancement function is possible from the energy sources [7]. Because injection of active power is used temporarily during transient, incorporating the stability en-hancement function in systems where active power injection is primarily used for other purposes [8] could be attractive.

In the specific case of shunt connected FACTS controllers [STATCOM and static var compensator (SVC)], first swing sta-bility and POD can be achieved by modulating the voltage at the point of common coupling (PCC) using reactive power in-jection. However, one drawback of the shunt configuration for this kind of applications is that the PCC voltage must be reg-ulated within specific limits (typically between 10% of the rated voltage), and this reduces the amount of damping that can be provided by the compensator. Moreover, the amount of in-jected reactive power needed to modulate the PCC voltage de-pends on the short circuit impedance of the grid seen at the con-nection point. Injection of active power, on the other hand, af-fects the PCC-voltage angle (transmission lines are effectively reactive) without varying the voltage magnitude significantly.

The control of STATCOM with energy storage (named here-after as E-STATCOM) for power system stability enhancement has been discussed in the literature [10]–[12]. However, the im-pact of the location of the E-STATCOM on its dynamic perfor-mance is typically not treated. When active power injection is used for POD, the location of the E-STATCOM has a significant impact on its dynamic performance. Moreover, the typical con-trol strategy of the device for POD available in the literature is similar to the one utilized for power system stabilizer (PSS) [9], where a series of wash-out and lead-lag filter links are used to generate the control input signals. This kind of control strategy is effective only at the operating point where the design of the filter links is optimized, and its speed of response is limited by the frequency of the electromechanical oscillations.

In this paper, a control strategy for the E-STATCOM when used for POD will be investigated. Thanks to the selected local signal quantities measured in the system, the control strategy optimizes the injection of active and reactive power to provide uniform damping at various locations in the power system. It will be shown that the implemented control algorithm is robust against system parameter uncertainties. For this, a modified re-cursive least square (RLS)-based estimation algorithm as de-scribed in [13], [14] will be used to extract the required control

International Journal of Research
Available at https://edupediapublications.org/journals
p-ISSN: 2348-6848
e-ISSN: 2348-795X
Volume 04 Issue 02
February 2017

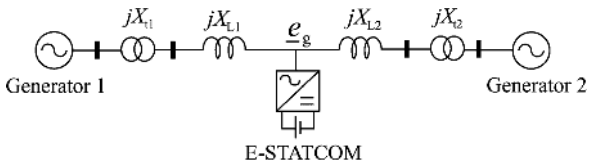

Fig. 1. Simplified two-machine system with E-STATCOM.

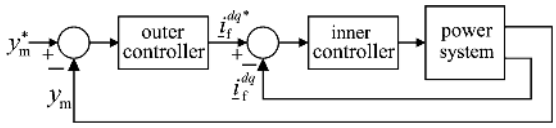

Fig. 2. Block diagram of the control of E-STATCOM.

signals from locally measured signals. Finally, the effectiveness of the proposed control strategy will be validated via simulation and experimental verification.

II. System Modeling for Controller Design

A simplified power system model, such as the one depicted in Fig. 1, is used to study the impact of the E-STATCOM on the power system dynamics. The investigated system approximates an aggregate model of a two-area power system, where each area is represented by a synchronous generator.

The synchronous generators are modeled as voltage sources of constant magnitude (V_{g1}, V_{g2}) and dynamic rotor angles $(\delta_{g1}, \delta_{g2})$ behind a transient reactance (X'_{d1}, X'_{d2}). The transmission system consists of two transformers represented by their equivalent leakage reactance (X_{t1}, X_{t2}) and a transmission line with equivalent reactance $(X_L = X_{L1} + X_{L2})$. The losses in the transmission system are neglected for simpler analytical expressions. If the mechanical damping in the generators is neglected, the overall damping for the investigated system is equal to zero. Therefore, the model is appropriate to allow a conservative approach of the impact of the E-STATCOM when used for stability studies [14]. For analysis purpose, the electrical connection point of the converter along the transmission line is expressed by the parameter a as

$$a = \frac{X_1}{(X_1 + X_2)} \tag{1}$$

where

$$X_1 = X'_{d1} + X_{t1} + X_{L1}$$
$$X_2 = X'_{d2} + X_{t2} + X_{L2}.$$

The outer control loop, which can be an ac voltage, dc-link voltage or POD controller, sets the reference current for the inner current controller. The generic measured signal de-pends on the type of outer loop control. The control algorithm is implemented in -reference frame where a phase-locked loop (PLL) [15] is used to track the grid-voltage angle from the grid-voltage vector . By synchronizing the PLL with the grid-voltage vector, the - a n d -components of the injected cur-rent (and) control the injected active and reactive power, and .

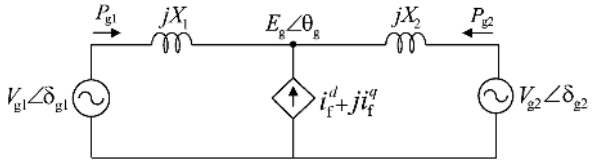

Fig. 3. Equivalent circuit for two-machine system with E-STATCOM.

respectively. In the notation in Fig. 2, the superscript "$*$" denotes the corresponding reference signals.

In this paper, the outer control loop is assumed to be a POD controller, and the detail of the block will be described in Section III. For this reason, we assume that the injected active and reactive powers in the steady state are zero. When designing a cascaded controller, the speed of outer control loop is typically selected to be much slower than the inner one to guarantee stability. This means that the current controller can be considered infinitely fast when designing the parameters of the outer controller loop. Therefore, the E-STATCOM can be modeled as a controlled ideal current source, as depicted in the equivalent circuit in Fig. 3, for analysis purpose.

The level of power oscillation damping provided by the converter depends on how much the active power output from the generators is modulated by the injected current, i_f. For the system in Fig. 3, the change in active power output from the generators due to injected active and reactive power from the E-STATCOM is calculated as in

$$\begin{aligned}
\Delta P_{g1,P} &\approx -\Gamma_P P_{inj}, \quad \Delta P_{g2,P} \approx -(1-\Gamma_P) P_{inj} \\
\Delta P_{g1,Q} &\approx \left[\frac{V_{g1}V_{g2}\sin(\delta_{g10}-\delta_{g20})a(1-a)}{E_{g0}^2}\right] Q_{inj} \\
\Delta P_{g2,Q} &\approx -\left[\frac{V_{g1}V_{g2}\sin(\delta_{g10}-\delta_{g20})a(1-a)}{E_{g0}^2}\right] Q_{inj}
\end{aligned} \tag{2}$$

where $(\Delta P_{g1,P}, \Delta P_{g2,P})$ and $(\Delta P_{g1,Q}, \Delta P_{g2,Q})$ represent the change in active power from the corresponding generators due to injected active power (P_{inj}) and reactive power (Q_{inj}), respectively. Γ_P, P_{inj}, and Q_{inj} are given by

$$\begin{aligned}
\Gamma_P &= \frac{\left([(1-a)V_{g1}]^2 + a(1-a)V_{g1}V_{g2}\cos(\delta_{g10}-\delta_{g20})\right)}{E_{g0}^2} \\
P_{inj} &\approx E_{g0} i_f^d \\
Q_{inj} &\approx -E_{g0} i_f^q.
\end{aligned} \tag{3}$$

The initial steady-state PCC voltage magnitude E_{g0} and generator rotor angles $(\delta_{g10}, \delta_{g20})$ correspond to the operating point where the converter is in idle mode. A derivation to the expressions in (2) is given in the Appendix.

Moreover, it can be understood from (2) that the effect of reactive power injection depends on the magnitude and direction of transmitted power from the generators.

III. POD Controller Design

The derivation of the POD controller from locally measured signals will be made in this section.

A. Derivation of Control Input Signals

Considering the simplified two-machine system in Fig. 1, the active power output from each generator should change in proportion to the change in its speed to provide damping [9]. From (2), it can be observed that the effect of the power injected by the compensator on the generator active power output highly depends on the parameter a, i.e., on the location of the E-STATCOM. Using the equivalent system in Fig. 3, a control input signal that contains information on the speed variation of the generators can be derived. When the E-STATCOM is not injecting any current, the variation of the locally measured signals, $\theta_{\rm g}$ and $P_{\rm tran}$ at different E-STATCOM connection points using the dynamic generator rotor angles $\delta_{\rm g1}$ and $\delta_{\rm g2}$ is given by

$$\theta_{\rm g} = \delta_{\rm g2} + \tan^{-1}\left[\frac{(1-a)V_{\rm g1}\sin(\delta_{\rm g1}-\delta_{\rm g2})}{(1-a)V_{\rm g1}\cos(\delta_{\rm g1}-\delta_{\rm g2})+aV_{\rm g2}}\right] \quad (4)$$

$$P_{\rm tran} = \frac{V_{\rm g1}V_{\rm g2}\sin(\delta_{\rm g1}-\delta_{\rm g2})}{X_1+X_2}. \quad (5)$$

From a small-signal point of view and under the assumption that the PCC-voltage magnitude along the line $E_{\rm g}$ does not change significantly, the required control input signals can be derived from the PCC-voltage phase and transmitted active power as [14]

$$\frac{d\theta_{\rm g}}{dt} \approx \Gamma_{\rm P}\omega_{\rm g0}\Delta\omega_{\rm g1} + (1-\Gamma_{\rm P})\omega_{\rm g0}\Delta\omega_{\rm g2} \quad (6)$$

$$\frac{dP_{\rm tran}}{dt} \approx \left\{\frac{V_{\rm g1}V_{\rm g2}\cos(\delta_{\rm g10}-\delta_{\rm g20})}{X_1+X_2}\right\}\omega_{\rm g0}[\Delta\omega_{\rm g1}-\Delta\omega_{\rm g2}] \quad (7)$$

where the constant $\Gamma_{\rm P}$ has been defined in the previous section. The nominal system frequency is represented by $\omega_{\rm g0}$ whereas $\Delta\omega_{\rm g1}$ and $\Delta\omega_{\rm g2}$ represent the speed variation of the generators in p.u. The electromechanical dynamics for each generator [i = 1, 2] is given by [9]

$$2H_{\rm gi}\frac{d\Delta\omega_{\rm gi}}{dt} = \Delta T_{\rm mi} - \Delta T_{\rm gi} - K_{\rm Dmi}\Delta\omega_{\rm gi} \quad (8)$$

where $H_{\rm gi}$, $\Delta\omega_{\rm gi}$, $\Delta T_{\rm mi}$, $\Delta T_{\rm gi}$, and $K_{\rm Dmi}$ represent inertia constant, speed variation, change in input torque, change in output torque and mechanical damping constant for the ith generator, respectively.

The derivative of the PCC-voltage phase and transmitted active power are both dependent on the speed variation of the generators. Moreover, the derivative of the PCC-voltage phase depends on the location of E-STATCOM, through the parameter $\Gamma_{\rm P}$, as well as the mechanical dynamics of the generators as shown in (8). This information will be exploited in the POD controller design.

For the two machine system in Fig. 1, damping is related to the variation of the speed difference between the two generators, $\Delta\omega_{\rm g12} = \Delta\omega_{\rm g1} - \Delta\omega_{\rm g2}$. From (2) and (3), it can be understood that the change in the output power from the generators due to injected active power is maximum when the compensator is installed at the generator terminals (i.e. $a = 0$ and $a = 1$). Assuming equal inertia constant for the two generators, no damping is provided by injection of active power at the electrical midpoint of the line (i.e., $a = 0.5$ for $H_{\rm g1} = H_{\rm g2}$) as the power output of the two generators is the same and the net impact is zero. At this location, the derivative of PCC-voltage phase is zero [see (6)]. This means that $d\theta_{\rm g}/dt$ scales the speed variation of the two generators depending on the location of E-STATCOM and its magnitude changes in proportion to the level of damping by active power injection. Therefore, $d\theta_{\rm g}/dt$ is an appropriate input signal for controlling the active power injection. On the other hand, it can be understood from (2) that the change in the output power from the generators due to injected reactive power is maximum at the electrical midpoint of the line (i.e., $a = 0.5$) and minimum at the generator terminals (i.e., $a = 0$ and $a = 1$). As the changes in the power output of the two generators are the same in magnitude and opposite in sign, a signal that varies linearly with the speed variation between the two generators, $\Delta\omega_{\rm g12}$ is an appropriate signal to control reactive power injection.

B. Estimation of Control Input Signals

This is achieved by the use of an estimation method based on a modified RLS algorithm. For reasons described in the previous subsection, the derivative of the PCC-voltage phase and the transmitted power should be estimated for controlling the ac-tive and reactive power injection, respectively. The aim of the algorithm is therefore to estimate the signal components that consist of only the low-frequency electromechanical oscillation in the measured signals and . By using a PLL with bandwidth much higher than the frequency of electromechan-ical oscillations, the derivative of the PCC-voltage phase can be obtained from the change in frequency estimate of the PLL . Therefore, the low-frequency electro-mechanical oscillation component can be extracted directly from the frequency estimate of the PLL. On the other hand, the derivative of transmitted power is estimated by extracting the low-frequency electromechanical oscillation component from the measured signal, and then applying a phase shift of

$$P_{\rm tran}$$

$\pi/2$ to the estimated oscillation frequency component.

From the estimated control input signals $\tilde{\omega}_{\rm g,osc} = d\tilde{\theta}_{\rm g,osc}/dt$ and $d\tilde{P}_{\rm tran,osc}/dt$, which contain only a particular oscillation frequency component, the reference injected active and reactive current components $(i_{\rm f}^{d*}, i_{\rm f}^{q*})$ from the E-STATCOM can be calculated to setup the POD controller as in Fig. 4. The terms $K_{\rm P}$ and $K_{\rm Q}$ represent proportional controller gains for the active and reactive current components, respectively.

To describe the estimation algorithm, an input signal y which could be either $\tilde{\omega}_{\rm g}$ or $P_{\rm tran}$, as shown in Fig. 4, is considered. Following a power system disturbance, y will consist of an average value that varies slowly and a number of low-frequency oscillatory components, depending on the number of modes that

International Journal of Research
Available at https://edupediapublications.org/journals
p-ISSN: 2348-6848
e-ISSN: 2348-795X
Volume 04 Issue 02
February 2017

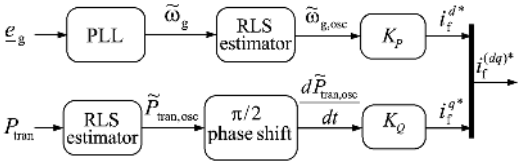

Fig. 4. Block diagram of the POD controller.

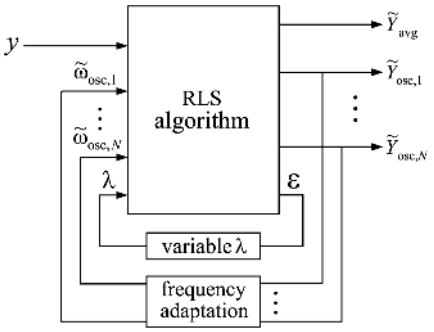

Fig. 5. Block diagram of the modified RLS estimator for multiple oscillation modes.

are excited by the disturbance. For simplicity, let us assume that there exist a single oscillatory component in the input signal. Therefore, the input signal consists of an average component $Y_{\rm avg}$ and an oscillatory component $Y_{\rm osc}$ which can be modeled as

$$y(t) = Y_{\rm avg}(t) + Y_{\rm ph}(t)\cos\left[\omega_{\rm osc}t + \varphi(t)\right] \tag{9}$$

where $Y_{\rm osc}$ is expressed in terms of its amplitude $(Y_{\rm ph})$, frequency $(\omega_{\rm osc})$ and phase (φ). The model in (9) is rewritten using the oscillation angle $\theta_{\rm osc}(t) = \omega_{\rm osc}t$ as

$$y(t) = Y_{\rm avg}(t) + Y_{{\rm ph},d}(t)\cos\left(\theta_{\rm osc}(t)\right) - Y_{{\rm ph},q}(t)\sin\left(\theta_{\rm osc}(t)\right)$$

where the terms $P_{{\rm ph},d}$ and $P_{{\rm ph},q}$ are given by

$$Y_{{\rm ph},d}(t) = Y_{\rm ph}(t)\cos\left(\varphi(t)\right) \quad Y_{{\rm ph},q}(t) = Y_{\rm ph}(t)\sin\left(\varphi(t)\right).$$

From an observation matrix Φ and measured input signal $y(t)$, the estimated state vector $\tilde{\mathbf{h}}$ is derived using the RLS algorithm in discrete time as [13], [14]

$$\tilde{\mathbf{h}}(k) = \tilde{\mathbf{h}}(k-1) + \mathbf{G}(k)\left[y(k) - \Phi(k)\tilde{\mathbf{h}}(k-1)\right] \tag{10}$$

with

$$\tilde{\mathbf{h}}(k) = \left[\tilde{Y}_{\rm avg}(k) \quad \tilde{Y}_{{\rm ph},d}(k) \quad \tilde{Y}_{{\rm ph},q}(k)\right]^{\rm T}$$
$$\Phi(k) = \left[1 \quad \cos\left(\theta_{\rm osc}(k)\right) \quad -\sin\left(\theta_{\rm osc}(k)\right)\right].$$

Calling $\mathbf{I}$ the identity matrix, the gain matrix $\mathbf{G}$ and covariance matrix $\mathbf{R}$ are calculated recursively starting with an initial invertible matrix $\mathbf{R}(0)$ as

$$\mathbf{G}(\mathrm{k}) = \mathbf{R}(\mathrm{k}-1)\Phi^{\rm T}(\mathrm{k})\left[\lambda + \Phi(\mathrm{k})\mathbf{R}(\mathrm{k}-1)\Phi^{\rm T}(\mathrm{k})\right]^{-1} \tag{11}$$

$$\mathbf{R}(\mathrm{k}) = \frac{\left[\mathbf{I} - \mathbf{G}(\mathrm{k})\Phi(\mathrm{k})\right]\mathbf{R}(\mathrm{k}-1)}{\lambda} \tag{12}$$

where λ represents the forgetting factor for the RLS algorithm such that $0 < \lambda \leq 1$. With $T_{\rm s}$ representing the sampling time, the steady-state bandwidth of the RLS $\alpha_{\rm RLS}$ and the estimation error $\epsilon(k)$ are given by [14]

$$\alpha_{\rm RLS} = \frac{(1-\lambda)}{T_{\rm s}}, \quad \epsilon(k) = y(k) - \Phi(k)\tilde{\mathbf{h}}(k-1).$$

Modification in the Conventional RLS Algorithm: The selection of $\alpha_{\rm RLS}$ is a tradeoff between a good selectivity for the estimator and its speed of response [13], [14]. With increasing estimation speed (decreasing), the frequency selectivity of the algorithm reduces. For this reason, the conventional RLS algorithm must be modified in order to achieve fast transient estimation without compromising its steady-state selectivity. In this paper, this is achieved with the use of variable forgetting factor as described in [13]. When the RLS algorithm is in steady-state, its bandwidth is determined by the steady-state forgetting factor $(\lambda_{\rm ss})$. If a rapid change is detected in the input (i.e., if the estimation error magnitude, $|\epsilon(k)|$ exceeds a predefined threshold), λ will be modified to a smaller transient forgetting factor $(\lambda_{\rm tr})$. Thus, by using a high-pass filter with time constant $\tau_{\rm hp}$, λ will be slowly increased back to its steady-state value $\lambda_{\rm ss}$.

Besides λ, the performance of the estimation method depends on accurate knowledge of the oscillating frequency, $\omega_{\rm osc}$. This frequency is dependent on the system parameters and its operating conditions. If the frequency content of the input changes, the estimator will give rise to a phase and amplitude error in the estimated quantities. Therefore, a frequency adaptation mechanism as described in [14] is implemented to track the true oscillation frequency of the input from the estimate of the oscillatory component, $\tilde{Y}_{\rm osc}$.

Modification for Multiple Oscillation Modes: The investigated control method has been derived under the assumption of a single oscillatory frequency component in the input signal. A brief description of how the proposed algorithm can be extended for multi-area system with multiple oscillation modes will be briefly presented here for future reference. Assuming that the input signal y contains N oscillatory components, (9) must be modified as

$$\begin{aligned} y(t) &= Y_{\rm avg}(t) + \sum_{i=1}^{N} Y_{{\rm osc},i} \\ &= Y_{\rm avg}(t) + \sum_{i=1}^{N} Y_{{\rm ph},i}(t)\cos\left[\omega_{{\rm osc},i}t + \varphi_i(t)\right] \end{aligned} \tag{13}$$

where the ith oscillation mode $Y_{{\rm osc},i}$ (with $i = 1, \ldots, N$) is expressed in terms of its amplitude $(Y_{{\rm ph},i})$, frequency $(\omega_{{\rm osc},i})$, and phase (φ_i). Using the model in (13)

be modified as described in Fig. 5. Thus, the POD controller in Fig. 4 can be modified accordingly to control each mode independently. Observe that the phase-shift applied for calculation of the reference currents depends on the investigated system and needs to be calculated for each oscillatory mode [9].

IV. Stability Analysis of System Model

The mathematical model of the system in Fig. 3 is developed in this section to investigate the performance of the POD controller using active and reactive power injection. Using the expressions in (6)–(7) for $d\theta_{\rm g}/dt$ and $dP_{\rm tran}/dt$, the injected currents are controlled as

$$i_{\rm f}^{\rm d} \approx K_{\rm P}\omega_{\rm g0}\left[\Gamma_{\rm P}\Delta\omega_{\rm g1} + (1-\Gamma_{\rm P})\Delta\omega_{\rm g2}\right] \tag{14}$$

$$i_{\rm f}^{\rm q} \approx K_{\rm Q}\omega_{\rm g0}\left\{\frac{V_{\rm g1}V_{\rm g2}\cos(\delta_{\rm g10}-\delta_{\rm g20})}{X_1+X_2}\right\}\left[\Delta\omega_{\rm g1}-\Delta\omega_{\rm g2}\right] \tag{15}$$

where the constant $\Gamma_{\rm P}$ is as defined in (3). Linearizing around an initial steady-state operating point, the small-signal dynamic model of the two-machine system with the E-STATCOM in per unit is developed as in

$$\frac{d}{dt}\begin{bmatrix}\Delta\omega_{\rm g1}\\ \Delta\delta_{\rm g12}\\ \Delta\omega_{\rm g2}\end{bmatrix} = \begin{bmatrix}\beta_{11} & \beta_{12} & \beta_{13}\\ \omega_{\rm g0} & 0 & -\omega_{\rm g0}\\ \beta_{31} & \beta_{32} & \beta_{33}\end{bmatrix}\begin{bmatrix}\Delta\omega_{\rm g1}\\ \Delta\delta_{\rm g12}\\ \Delta\omega_{\rm g2}\end{bmatrix} + \begin{bmatrix}\frac{1}{2H_{\rm g1}} & 0\\ 0 & 0\\ 0 & \frac{1}{2H_{\rm g2}}\end{bmatrix}\begin{bmatrix}\Delta T_{\rm m1}\\ \Delta T_{\rm m2}\end{bmatrix} \tag{16}$$

where $\Delta\delta_{\rm g12} = \Delta\delta_{\rm g1} - \Delta\delta_{\rm g2}$ represents the rotor angle difference between the two generators and other signals as defined previously. Assuming no mechanical damping and the initial steady-state speed of the generators set to $\omega_{\rm g0}$, the constants are derived as in

$$\begin{bmatrix}\beta_{11}\\ \beta_{12}\\ \beta_{13}\\ \beta_{31}\\ \beta_{32}\\ \beta_{33}\end{bmatrix} = \begin{bmatrix}\frac{\omega_{\rm g0}\left(K_{\rm P}E_{\rm g0}\Gamma_{\rm P}^2+K_{\rm Q}\Gamma_{\rm Q}\right)}{2H_{\rm g1}}\\ -\frac{V_{\rm g1}V_{\rm g2}\cos(\delta_{\rm g10}-\delta_{\rm g20})}{2H_{\rm g1}(X_1+X_2)}\\ \frac{\omega_{\rm g0}(K_{\rm P}E_{\rm g0}\Gamma_{\rm P}(1-\Gamma_{\rm P})-K_{\rm Q}\Gamma_{\rm Q})}{2H_{\rm g1}}\\ \frac{\omega_{\rm g0}(K_{\rm P}E_{\rm g0}\Gamma_{\rm P}(1-\Gamma_{\rm P})-K_{\rm Q}\Gamma_{\rm Q})}{2H_{\rm g2}}\\ \frac{V_{\rm g1}V_{\rm g2}\cos(\delta_{\rm g10}-\delta_{\rm g20})}{2H_{\rm g2}(X_1+X_2)}\\ \frac{\omega_{\rm g0}\left(K_{\rm P}E_{\rm g0}(1-\Gamma_{\rm P})^2+K_{\rm Q}\Gamma_{\rm Q}\right)}{2H_{\rm g2}}\end{bmatrix} \tag{17}$$

where $\Gamma_{\rm Q}$ is given by

$$\Gamma_{\rm Q} = \frac{[V_{\rm g1}V_{\rm g2}]^2\sin\left(2(\delta_{\rm g10}-\delta_{\rm g20})\right)a(1-a)}{2E_{\rm g0}(X_1+X_2)}. \tag{18}$$

The terms β_{12} and β_{32} represent the synchronizing torque coefficients resulting from the selected operating point and the contribution of the E-STATCOM is zero. The terms β_{11} and β_{33} determine the damping torque coefficient provided by the E-STATCOM with respect to the change in speed of the respective generator. To provide positive damping, β_{11} and β_{33} should be negative. For this, the sign of $K_{\rm P}$ should be negative and the sign of $K_{\rm Q}$ should be chosen based on the sign of $\Gamma_{\rm Q}$. For a transmitted power from Generator 1 to Generator 2, $\Gamma_{\rm Q}$ will be positive and the sign of $K_{\rm Q}$ should be negative. For a transmitted power in the other direction, the sign of $K_{\rm Q}$ should be opposite. The terms β_{13} and β_{31} are the cross coupling terms between the two generator speed variations.

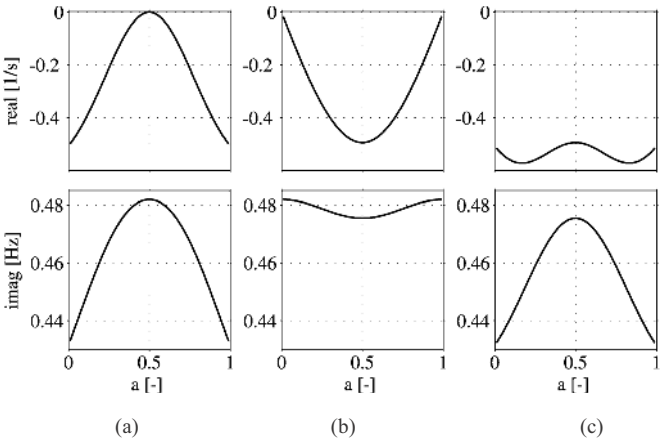

Fig. 6. Real and imaginary part of the complex conjugate poles versus position. (a) Active power injection. (b) Reactive power injection. (c) Active and reactive power injection. [$K_{\rm P} = -0.08, K_{\rm Q} = -0.34, P_{\rm tran} =$ 0.4444 p.u.].

With active power injection only ($K_{\rm Q} = 0$), the cross coupling terms reduce the damping as the speed variation of the generators will be opposite at the oscillatory frequency. At the mass-scaled electrical midpoint of the line where $d\theta_{\rm g}/dt = 0$, the damping that can be provided by $P_{\rm inj}$ is zero. Therefore, the active power injected by the E-STATCOM at this location is set to zero by the control algorithm. When moving away from this point towards the generator terminals, $\Gamma_{\rm P}$ increases and at the same time the cross coupling terms decrease. This enhances the damping that can be provided by active power injection and therefore the amount of injected active power is increased. In the case of reactive power injection only ($K_{\rm P} = 0$), positive damping is provided by the cross coupling terms and maximum damping is provided at the electrical midpoint of the line (i.e., $a = 0.5$ for a symmetrical system) where $\Gamma_{\rm Q}$ magnitude is maximum.

As an example for the analysis in this section, a hypothetical 20/230 kV, 900 MVA transmission system similar to the one in Fig. 1 with a total series reactance of 1.665 p.u. and inertia constant of the generators $H_{\rm g1} = H_{\rm g2} = 6.5$ s is considered. The leakage reactance of the transformers and transient impedance of the generators are 0.15 p.u. and 0.3 p.u., respectively. The movement of the poles for the system as a function of the E-STATCOM location is shown in Fig. 6. With the described control strategy, injected active power is zero at the point where the effect of active power injection on damping is zero. This is at the electrical midpoint of the line. On the other hand, at the same location damping by reactive power injection is maximum. The reverse happens at either end of the generators.

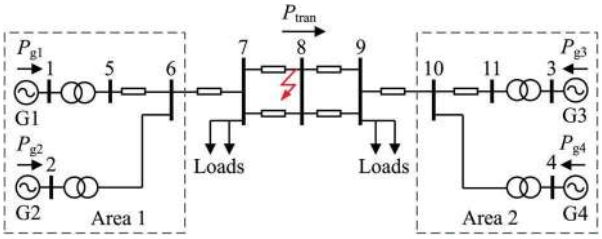

Fig. 7. Simplified two-area four machine power system.

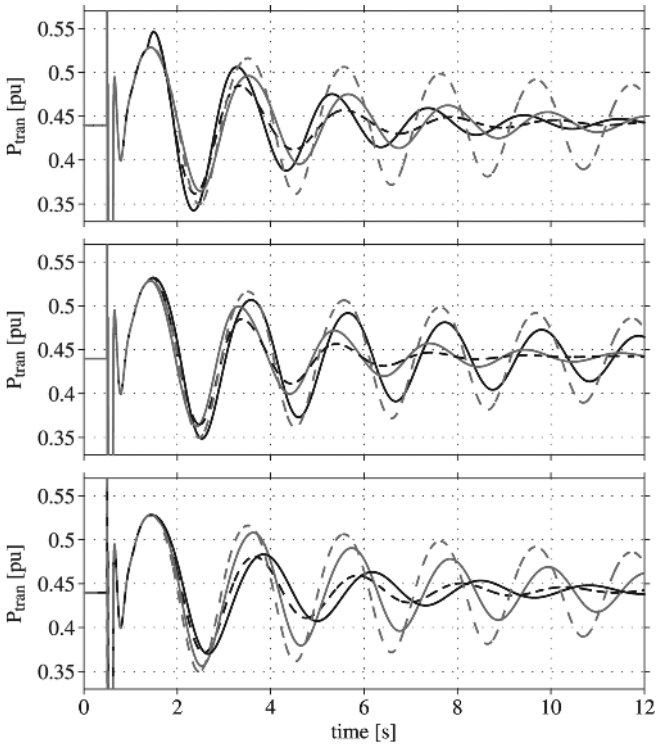

Fig. 8. Measured transmitted active power output following a three-phase fault with E-STATCOM connected at bus 7 (top), bus 8 (middle), and bus 9 (bottom). POD by $P_{\rm inj}$ only (black solid), $Q_{\rm inj}$ only (gray solid), both $P_{\rm inj}$, $Q_{\rm inj}$ (black dashed), and no POD (gray dashed).

V. Simulation Results

The POD controller described in Section III is here verified via PSCAD/EMTDC simulation using the well known two-area four-machine system in Fig. 7. The implemented system is rated 20/230 kV, 900 MVA and the parameters for the generators and transmission system together with the loading of the system are given in detail in [9]. The system is initially operating in steady-state with a transmitted active power, $P_{\rm tran} = 400$ MW from area 1 to area 2. A three-phase fault is applied to the system on one of the transmission lines between bus 7 and bus 8. The fault is cleared after 120 ms by disconnecting the faulted line. Due to the applied disturbance, a poorly damped oscillation is obtained after the fault clearing.

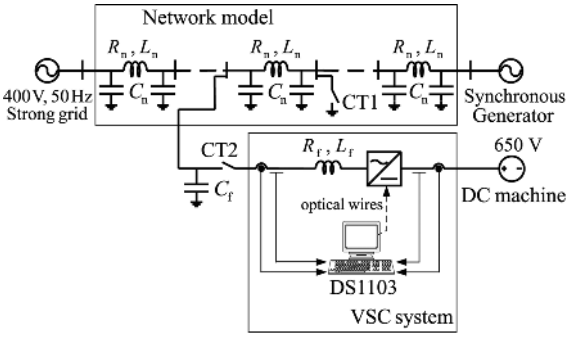

Fig. 9. Single-line diagram of the laboratory setup.

(a) (b)

Fig. 10. Photograph of the laboratory setup. (a) Analog transmission-line model. (b) Generator system.

is achieved by active power injection (see Fig. 8, black solid plots). With respect to reactive power injection, maximum damping action is provided when the E-STATCOM is connected close to the electrical midpoint of the line and the level of damping decreases when moving away from it (see Fig. 8, gray solid plots). Because of a good choice of signals for controlling both active and reactive power injection, effective power oscillation damping is provided by the E-STATCOM irrespective of its location in the line (see Fig. 8, black dashed plots).

VI. Experimental Verification

To validate the results obtained via simulation for the POD controller performance by E-STATCOM, the obtained experimental results will be presented in this section.

A. Laboratory Setup

The schematic of the laboratory setup is shown in Fig. 9, while Fig. 10 shows a photograph of the actual transmission system model. The system consists of a 75-kVA, 400-V synchronous generator connected to a stiff ac grid through a transmission-line model. A voltage source converter (VSC) system can be connected at various locations of the transmission line.

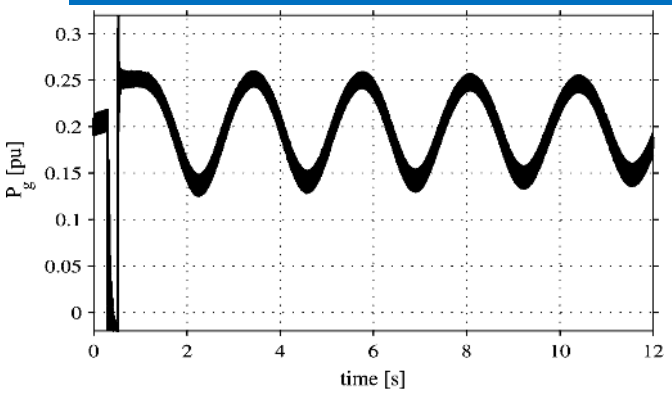

Fig. 11. Measured transmitted active power from the generator. A three-phase fault is applied and cleared after 250 ms.

dc machine rated 700 V and 60 A. The dc machine is equipped with field control and the terminal dc voltage is controlled to 650 V for all of the experiments. The dc machine will act as the energy source providing active power injection capability to the VSC. Therefore, the VSC with the dc machine is considered as an E-STATCOM.

2) Network Model: The network model is a down-scaled version of an actual Swedish 400 kV transmission system with the model rated at 400 V, 50 Hz. The transmission-line model consists of six identical Π sections (with parameters $L_{\mathrm{n}} = 2.05$ mH, $R_{\mathrm{n}} = 0.05\ \Omega$ and $C_{\mathrm{n}} = 46\ \mu$F), each corresponding to a portion of 150 km of the actual line [16]. As shown in Fig. 9, faults can be applied to the transmission system using the contactor (CT1).

3) Synchronous Generator: A photograph of the generator system which represents an actual model of the large Harsprånget hydro power plant, situated by the Luleå river in northern Sweden is shown in Fig. 10. The synchronous generator has an inertia constant of 5.6 s, and it is driven by an 85-kW dc motor [16].

B. Experimental Verification of Modified RLS Estimator

In order to create a power oscillation in the system, a three-phase fault has been applied in the middle of the transmission line. The fault clearing time is 250 ms. The measured output power from the generator $P_{\mathrm{g}}(t)$ as shown in Fig. 11 is then used as an input to test the performance of the algorithm to estimate the low-frequency electromechanical oscillation component. The actual oscillation frequency of the measured signal $P_{\mathrm{g}}(t)$ is about 0.42 Hz. This low oscillation frequency highlights the importance of the adopted estimation method, since the classical approaches based on filters would require low bandwidth, resulting in a reduction in the estimation speed [14]. To investigate the robustness of the algorithm against system parameter changes, an initial oscillatory frequency of 0.6 Hz is assumed in the estimation.

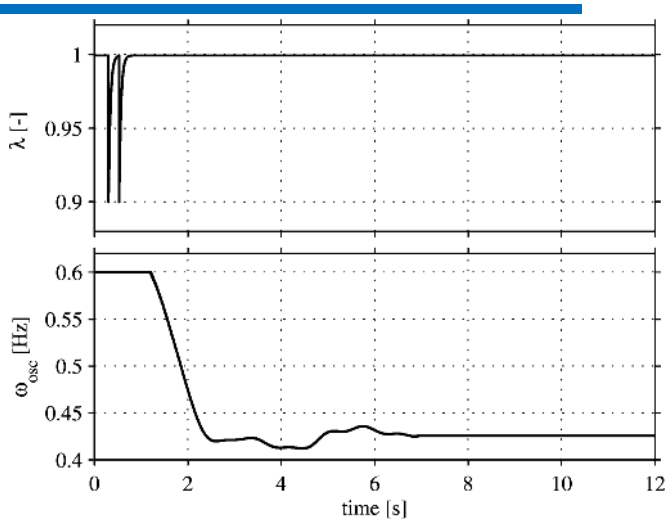

Fig. 12. Modified RLS-based estimator. Variation of forgetting factor λ (top) and estimate of oscillation frequency $\tilde{\omega}_{\mathrm{osc}}$ (bottom).

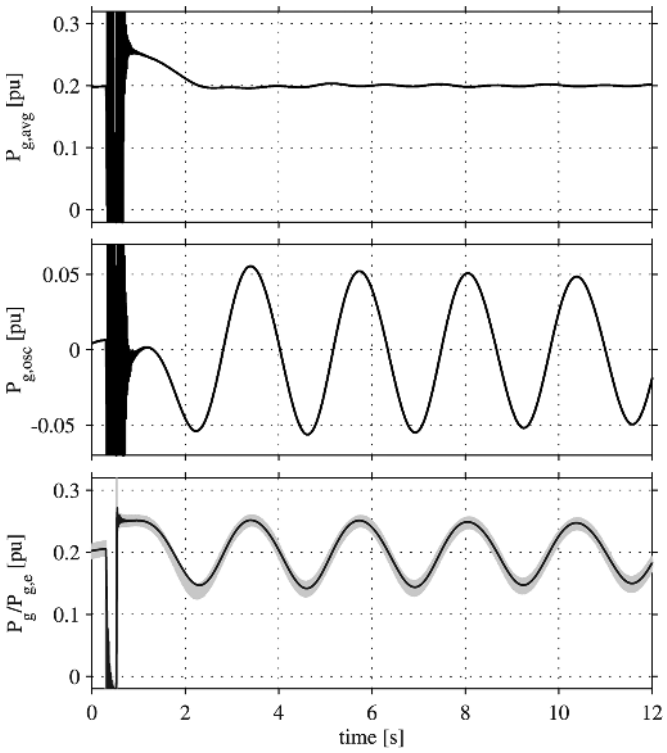

Fig. 13. Estimate for the average and oscillatory component. Top: estimated average component. Middle: estimated oscillatory component. Bottom: measured generator active power signal (gray line) and estimated signal (black line).

thanks to the variation of λ, very fast transient performance is achieved. The frequency adaptation ensures a correct extraction of the magnitude and phase of the oscillatory component which is a crucial point in the POD application.

C. Experimental Verification of POD Controller by E-STATCOM

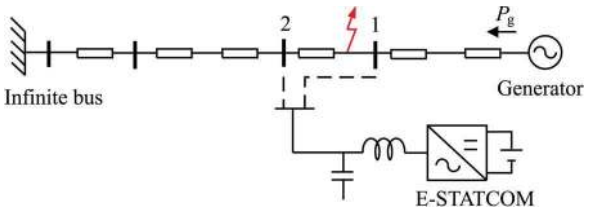

Fig. 14. Single-line diagram of the laboratory setup for POD.

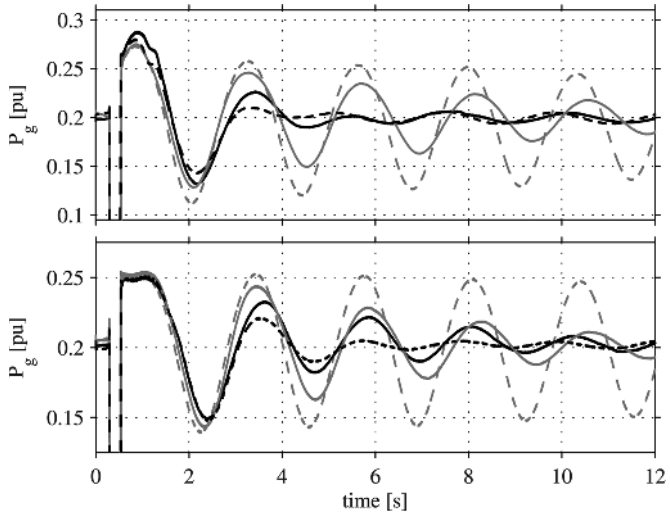

Fig. 15. Measured generator active power output following a three-phase fault with E-STATCOM connected at bus 1 (top) and bus 2 (bottom). POD by P_{inj} only (black solid line), Q_{inj} only (gray solid line), both P_{inj}, Q_{inj} (black dashed line) and no POD (gray dashed line).

here is a Proportional-Integral based vector controller. It is designed based on the internal model control approach. The bandwidth of the controller is chosen as 2500 rad/s, and the detail of the implementation can be found in [14]. To verify the POD controller performance, the setup in Fig. 9 which represents a single-machine infinite bus system with E-STATCOM is used. The single-line diagram of the setup is shown in Fig. 14, where the possible connection buses of the E-STATCOM are marked as 1 and 2. For the tests, the gain K_{Q} is chosen to get a damping ratio of 10% at bus 2 when reactive power is used for POD. For a fair comparison, the gain K_{P} is then adjusted to get a similar order of maximum active and reactive power injection for the tests. Once the values for the gains are selected, they are kept constant for all the experiments.

First, the power oscillation damping controller is tested with two connection points of the E-STATCOM as shown in Fig. 14. For this test, knowledge of the oscillatory frequency in the transmitted active power has been considered. As before, a three-phase fault is applied at bus 1 and the fault is cleared after 250 ms. The performance of the E-STATCOM for POD using the control strategy described in Section III is shown in Figs. 15 and 16. Observe that, to facilitate the comparison, the presented measured signals have been fil t e r e d t o r e m o v e n o i s e a n d h i g h - frequency harmonic components.As described in the small-signal analysis in Section IV, the injected active power decreases with

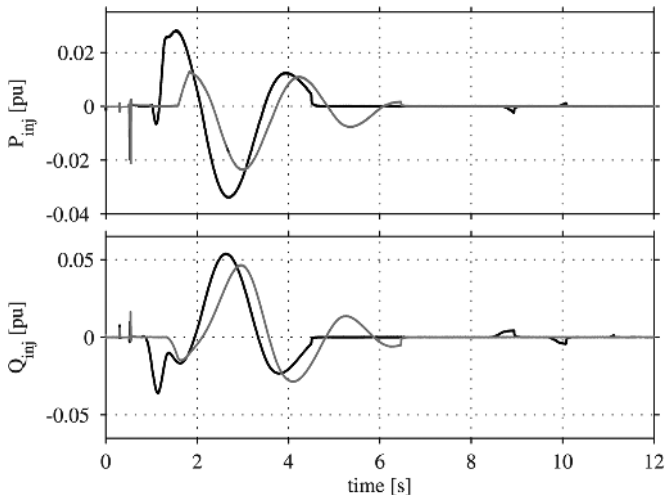

Fig. 16. Injected active and reactive power with E-STATCOM connected at bus 1 (black line) and bus 2 (gray line). Active power injection (top) and reactive power injection (bottom); both P_{inj} and Q_{inj} used for POD.

the distance from the generator where its impact to provide damping decreases (see Fig. 16). A better damping with active power injection is obtained when the E-STATCOM is closer to the generator, in this case at bus 1 (see Fig. 15). With respect to reactive power injection, the damping provided by the compensator increases when moving closer to the electrical midpoint. As the transmitted power P_{g} is used to control reactive power, the same amount of injected reactive power is used at the two locations and a better damping action is provided close to the electrical midpoint of the line, in this case at bus 2. With a proper choice of control signals for injection of active and reactive power, effective power oscillation damping is provided by the E-STATCOM at both connection points of the compensator as shown in Fig. 15 (black dashed curves).

To test the dynamic performance of the investigated POD controller in case of system parameter changes, a second set of experiments has been carried out assuming an oscillation frequency of 0.9 Hz, where the actual measured oscillation frequency is 0.42 Hz. This means that an error of 100% in the estimated oscillation frequency is here considered. Fig. 17 compares the performance of the POD controller with and without the oscillation frequency adaptation in the RLS estimator. In both cases, the E-STATCOM is connected at bus 2 and injection of active and reactive power is used for POD. By using the frequency adaption as described in Section III-B, the phase of the oscillatory component in the input signal is correctly estimated, thus providing an effective damping. This is advantageous when compared to the classical approaches, where the correct phase shift is provided in the estimation only at a particular oscillation frequency. As shown in Fig. 17 (gray solid plots), if the POD controller is not adapted to changes in the system, its performance is significantly reduced. This is also shown in Fig. 18, where the total energy exchange (W_{total}) between the E-STATCOM and the grid until the oscillations are completely damped for the two cases is displayed. This results in an uneconomical use of the energy

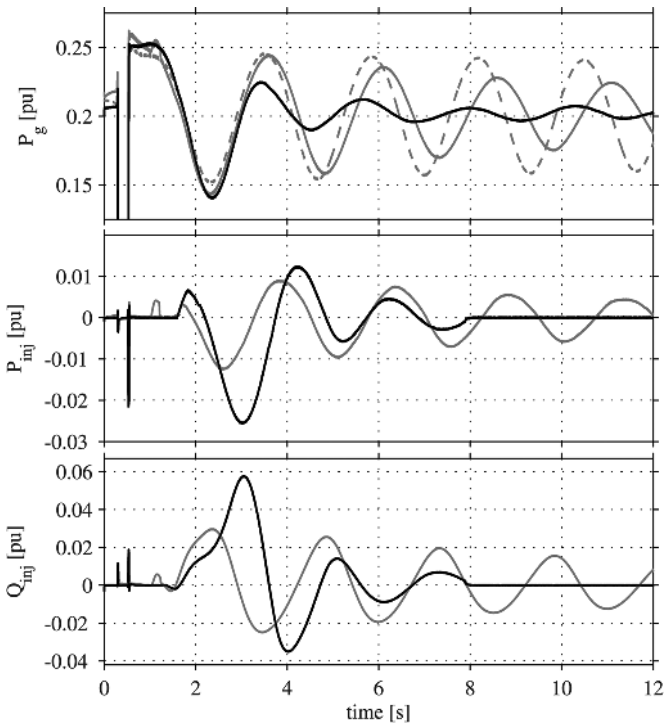

Fig. 17. Top: measured generator output power with frequency adaptation (black solid), without frequency adaptation (gray solid line) and with no POD (gray dashed line). Middle: injected active power with frequency adaptation (black line) and without frequency adaptation (gray line). Bottom: injected reactive power with frequency adaptation (black) and without frequency adaptation (gray line).

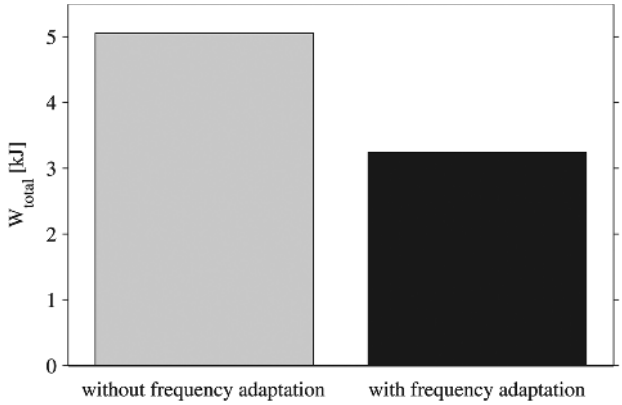

Fig. 18. Total energy exchange to damp oscillations with and without frequency adaptation.

storage. Observe that in order to avoid continuous injection of active and reactive power, the POD controller implemented in the laboratory sets the reference active and reactive currents to zero when the amplitude of the oscillatory signal goes below a pre-defined threshold. Here, this threshold is set to 0.005 pu. As an example, it is clear from Fig. 17 (middle and bottom plots) that, when the adaptive POD controller is used, the amplitude of the power oscillation crosses this threshold at 8 s. As a result, the active and reactrive powers injected by the compensator become zero.

VII. Conclusion

An adaptive POD controller by E-STATCOM has been developed in this paper. For this, a modified RLS algorithm has been used for estimation of the low-frequency electromechanical oscillation components from locally measured signals during power system disturbances. The estimator enables a fast, selective and adaptive estimation of signal components at the power oscillation frequency. The dynamic performance of the POD controller to provide effective damping at various connection points of the E-STATCOM has been validated through simulation as well as experimental verification. The robustness of the control algorithm against system parameter changes has also been proven through experimental tests. Furthermore, using the frequency variation at the E-STATCOM connection point as the input signal for the active power modulation, it has been shown that active power injection is minimized at points in the power system where its impact on POD is negligible. This results in an optimal use of the available energy source.

Appendix

Here, the relation between the change in active power output from the generators and the active and reactive power injected by the E-STATCOM will be derived. With the notations given in Fig. 3, the power output of Generator 1 is given by

$$P_{\mathrm{g1}} = \frac{V_{\mathrm{g1}} E_{\mathrm{g}} \sin(\delta_{\mathrm{g1}} - \theta_{\mathrm{g}})}{X_1}. \tag{19}$$

From a small-signal point of view, the change in PCC voltage $\Delta \underline{E}_{\mathrm{g}}$ from its initial steady-state value $E_{\mathrm{g0}} \angle \theta_{\mathrm{g0}}$ due to injection of active and reactive current is given by

$$\Delta \underline{E}_{\mathrm{g}} = j \frac{X_1 X_2}{X_1 + X_2} \left(i_{\mathrm{f}}^d + j i_{\mathrm{f}}^q \right) = -X_{\mathrm{th}} i_{\mathrm{f}}^q + j X_{\mathrm{th}} i_{\mathrm{f}}^d \tag{20}$$

where X_{th} represents the Thevenin equivalent impedance at the PCC. Equation (20) can be expressed in terms of amplitude and phase change as

$$\Delta E_{\mathrm{g}} \approx -X_{\mathrm{th}} i_{\mathrm{f}}^q, \quad \Delta \theta_{\mathrm{g}} \approx \frac{X_{\mathrm{th}} i_{\mathrm{f}}^d}{E_{\mathrm{g0}}}. \tag{21}$$

The change in active power output of Generator 1 due to injection of active and reactive current from the E-STATCOM is derived from (19)–(21) as

$$\Delta P_{\mathrm{g1,P}} \approx -V_{\mathrm{g1}} \cos(\delta_{\mathrm{g10}} - \theta_{\mathrm{g0}}) X_{\mathrm{th}} i_{\mathrm{f}}^d / X_1 \tag{22}$$

$$\Delta P_{\mathrm{g1,Q}} \approx -V_{\mathrm{g1}} \sin(\delta_{\mathrm{g10}} - \theta_{\mathrm{g0}}) X_{\mathrm{th}} i_{\mathrm{f}}^q / X_1. \tag{23}$$

In steady state, i.e., when the E-STATCOM is in idle mode, the PCC voltage $\underline{E}_{\mathrm{g0}}$ can be expressed as

$$E_{\mathrm{g0}} \angle \theta_{\mathrm{g0}} = (1-a) V_{\mathrm{g1}} \angle \delta_{\mathrm{g10}} + a V_{\mathrm{g2}} \angle \delta_{\mathrm{g20}} \tag{24}$$

where a is the relative electrical location of the E-STATCOM as defined in (1).

Substituting (24) into (22) and (23) and defining Γ_{P}, P_{inj} and Q_{inj} as in (3), the change in active power output from Generator 1 due to injection of active and reactive power from the E-STATCOM given in (2) can be derived. By conservation of energy, the expression for the change in active power output

from Generator 2 due to injection of active and reactive power is calculated as $\Delta P_{g2P} = -P_{inj} - \Delta P_{g1P}$ and $\Delta P_{g2Q} = -\Delta P_{g1Q}$.

REFERENCES

[1] N. G. Hingorani and L. Gyugyi, *Understanding FACTS. Concepts and Technology of Flexible AC Transmission Systems*. New York, NY, USA: IEEE, 2000.
[2] G. Cao, Z. Y. Dong, Y. Wang, P. Zhang, and Y. T. Oh, "VSC based STATCOM controller for damping multi-mode oscillations," in *Proc. IEEE Power and Energy Soc. General Meeting—Conversion and Delivery of Electrical Energy in the 21st Century*, Jul. 2008, pp. 1–8.
[3] M. Zarghami and M. L. Crow, "Damping inter-area oscillations in power systems by STATCOMs," in *Proc. 40th North Amer. Power Symp.*, Sep. 2008, pp. 1–6.
[4] Z. Yang, C. Shen, L. Zhang, M. L. Crow, and S. Atcitty, "Integration of a statcom and battery energy storage," *IEEE Trans. Power Syst.*, vol. 16, no. 2, pp. 254–260, May 2001.
[5] A. Arulampalam, J. B. Ekanayake, and N. Jenkins, "Application study of a STATCOM with energy storage," *Proc. Inst. Electr. Eng.—Gener., Transm. and Distrib.*, vol. 150, pp. 373–384, July 2003.
[6] N. Wade, P. Taylor, P. Lang, and J. Svensson, "Energy storage for power flow management and voltage control on an 11 kV UK distribution network," Prague, Czech Republic, CIRED paper 0824, Jun. 2009.
[7] A. Adamczyk, R. Teodorescu, and P. Rodriguez, "Control of full-scale converter based wind power plants for damping of low frequency system oscillations," in *Proc. IEEE PowerTech*, Trondheim, Norway, Jun. 2011, pp. 1–7.
[8] H. Xie, "On power-system benefits, main-circuit design, control of Statcoms with energy storage," Ph.D. dissertation, Dept. Electr. Energy Conversion, Royal Inst. Technol., Stockholm, Sweden, 2009.
[9] P. Kundur, *Power System Stability and Control*. New York, NY, USA: McGraw-Hill, 1994.
[10] K. Kobayashi, M. Goto, K. Wu, Y. Yokomizu, and T. Matsumura, "Power system stability improvement by energy storage type STATCOM," in *Proc. IEEE Power Tech Conf.*, Bologna, Italy, Jun. 2003, vol. 2, DOI 10.1109/PTC.2003.1304302.
[11] L. Zhang and Y. Liu, "Bulk power system low frequency oscillation suppression by FACTS/ESS," in *Proc. IEEE PES Power Syst. Conf. Exp.*, Oct. 2004, pp. 219–226.
[12] A. Arsoy, L. Yilu, P. F. Ribeiro, and F. Wang, "Power converter and SMES in controlling power system dynamics," in *Proc. Ind. Appl. Conf.*, Oct. 2000, vol. 4, pp. 2051–2057.
[13] M. Beza and M. Bongiorno, "A fast estimation algorithm for low-frequency oscillations in power systems," in *Proc. 14th Eur. Conf. Power Electron. Appl.*, Sep. 2011, pp. 1–10.
[14] M. Beza, "Control of energy storage equipped shunt-connected converter for electric power system stability enhancement," Licentiate Thesis, Dept. Energy and Environment, Chalmers Univ. of Technol., Gothenburg, Sweden, 2012, .
[15] L. Ängquist and M. Bongiorno, "Auto-normalizing phase-locked loop for grid-connected converters," in *Proc. IEEE Energy Conv. Congress*

Profile of Authors

SHAIK MOHAMAD RAFI

Student, Sana Engineering College, Kodad, Telangana, India

VORUGANTI BHARATH KUMAR

Student, Sana Engineering College, Kodad, Telangana, India

MAHAMAD SAMREEN SULTHANA

Guide, Sana Engineering College, Kodad, Telangana, India